Published in final edited form as:
J Nucl Med. 2010 July ; 51(7): 1107–1115. doi:10.2967/jnumed.110.075259.

Molecular Imaging of Matrix Metalloproteinase Activation to Predict Murine Aneurysm Expansion in vivo

Mahmoud Razavian, PhD[1,2,*], **Jiasheng Zhang, MD**[1,2,*], **Lei Nie, PhD**[1,2], **Sina Tavakoli, MD**[1,2], **Niema Razavian**[1,2], **Lawrence W. Dobrucki, PhD**[1], **Albert J. Sinusas, MD**[1], **D. Scott Edwards, PhD**[3], **Michael Azure, PhD**[3], and **Mehran M. Sadeghi, MD**[1,2]

[1] Cardiovascular Molecular Imaging Laboratory, Section of Cardiovascular Medicine, Yale University School of Medicine, New Haven, CT

[2] VA Connecticut Healthcare System, West Haven, CT

[3] Lantheus Medical Imaging, North Billerica, MA

Abstract

Rupture and dissection are major causes of morbidity and mortality in arterial aneurysm and occur more frequently in rapidly expanding aneurysms. Current imaging modalities provide little information on aneurysm beyond size. MMP activation plays a key role in the pathogenesis of aneurysm. We investigated whether imaging matrix metalloproteinase (MMP) activation in aneurysm helps predict its propensity to expansion.

Methods and Results—Using a model of carotid aneurysm in apolipoprotein $E^{-/-}$ mice we demonstrate that several MMPs are expressed with distinct temporal patterns in aneurysm. Radiotracers with specificity for activated MMPs were used to detect and quantify MMP activation by microSPECT/CT imaging in vivo. Significant focal uptake was observed in aneurysmal carotid arteries, peaking at 4 weeks after aneurysm induction. Tracer uptake was confirmed by autoradiography and gamma-well counting, and specificity was demonstrated using excess unlabeled precursor and a specific MMP inhibitor. In a group of animals imaged serially at 2 and 4 weeks after aneurysm induction, MMP tracer uptake at 2 weeks correlated well with the vessel area assessed by histology at 4 weeks.

Conclusions—Molecular imaging of MMP activation is a useful experimental, and potentially clinical, tool to non-invasively predict an aneurysm's propensity to expansion in vivo.

Keywords

Nuclear imaging; matrix metalloproteinases; aneurysm

Introduction

Aneurysm, focal dilation of large arteries, is a prevalent disease of various vascular beds, including abdominal and thoracic aorta, iliac arteries, and popliteal arteries. The

Corresponding Author: (reprints are not available): Mehran M. Sadeghi, M.D. VA Connecticut Healthcare System, 950 Campbell Avenue, 111B, West Haven, CT 06516, Fax: 203-937 3884, Phone: 203-932 5711 x3398, Mehran.sadeghi@yale.edu.
*these authors contributed equally to this work
1st co-authors: Mahmoud Razavian and Jiasheng Zhang, VA Connecticut Healthcare System, 950 Campbell Avenue, 111B, West Haven, CT 06516, Fax: 203-937 3884, Phone: 203-932 5711 x5705, Mahmoud.razavian@yale.edu, Jiasheng.zhang@yale.edu

Disclosures: D. Scott Edwards and Michael Azure are employees of Lantheus Medical Imaging. Albert Sinusas and Mehran Sadeghi receive experimental tracers from Lantheus Medical Imaging. In addition, Albert Sinusas has received research grants from Lantheus Medical Imaging.

pathogenesis of aneurysm commonly involves inflammation, protease activation, extracellular matrix remodeling and vascular smooth muscle cell (VSMC) dysfunction and apoptosis, which ultimately lead to the weakening of the vessel wall and arterial expansion under the influence of mechanical forces (1,2). Rupture, dissection, and distal embolization are frequent and highly morbid complications of aneurysm. While size is the best predictor of the risk of complications, rapid expansion also increases an aneurysm's propensity to rupture or dissection. Current practice guidelines recommend surgical treatment for large aneurysms and monitoring by serial imaging for smaller aneurysms (3). However, a large number of complications occur in smaller aneurysms which do not meet the criteria for surgical repair (4,5). Prospective identification of such smaller aneurysms that are at high risk for complications can tilt the risk-benefit balance towards early treatment and reduce aneurysm morbidity and mortality.

Matrix metalloproteinases (MMPs), a multi-gene family of endopeptidases that selectively digest individual components of the extracellular matrix, play a key role in the pathogenesis of aneurysm and its complications, rupture and dissection (6–9). MMPs are biosynthesized as inactive secreted or transmembrane proenzymes which are activated through enzymatic cleavage of the propeptide domain. This exposes a catalytic domain which may be targeted for imaging using specific probes (10). Imaging targeted at molecular markers of disease activity provides a unique opportunity to elicit information on the pathogenic process in vivo. The central role of MMP-mediated matrix remodeling in arterial aneurysm raises the possibility that MMP-targeted imaging may detect an aneurysm's propensity to expansion in vivo. Here, we use a family of radiotracers with specificity for activated MMP catalytic domain (11) to image MMP activation in murine carotid aneurysm in vivo. We show that MMP-targeted imaging reflects MMP activity detected by zymography in the vessel wall and demonstrate that molecular imaging of MMP activation in vivo provides unique information on aneurysm's molecular properties that are related to expansion.

Methods

Reagents

Reagents were from Sigma (St Louis, MI), unless otherwise specified. RP782, an ^{111}In-labeled tracer with specificity for activated MMPs and the precursor for its ^{99}Tc-labeled homologue, RP805 (11) were provided by Lantheus Medical Imaging (North Billerica, MA). RP805 radiolabeling was performed according to the manufacturer's instructions. The structure, binding characteristics and biodistribution in mouse of MMP tracers were previously reported (11–13).

Animal model

Arterial aneurysm was induced by exposing the left common carotid artery of apolipoprotein E (apoE) $^{-/-}$ mice to calcium chloride as described previously with modifications (14). This model reliably leads to the development of a large aneurysm in the great majority of animals. Briefly, 4- to 6-week old female apoE$^{-/-}$ mice (Jackson Laboratory, Bar Harbor, ME, n=96) were fed high-cholesterol chow (1.25% cholesterol, Harlan Teklad, Madison, WI) ad libitum. After 1 week, the carotid arteries were exposed by blunt-end dissection under anesthesia (ketamine 100 mg/kg and xylazine 10 mg/kg, ip). The left common carotid artery just below carotid bifurcation was adventitially exposed to a 10% solution of $CaCl_2$ for 20 minutes. The opposite carotid artery was exposed to normal saline and served as control for imaging studies. Ibuprofen (0.11 mg/kg/day, po) was used for postoperative analgesia. Experiments were performed according to regulations of Yale University's Animal Care and Use Committee.

Histology, morphometry, and immunofluorescent staining

Animals were anesthetized at 2, 4 or 8 weeks after surgery. After perfusion with normal saline, carotid arteries were harvested, embedded in OCT compound, snap-frozen, and stored at −80°C until further use. Elastic van Gieson and immunostaining were performed according to standard protocols on 5 μm-thick cryostat sections. For morphometric analysis, microscopic measurements were performed on cryostat sections with NIH ImageJ software (National Institutes of Health, Bethesda, MD), as previously described (15). The area within the external elastic lamina (total vessel area) was calculated by averaging measurements from ten sections at 200μm intervals from 200μm to 2000μm below carotid bifurcation. For immunostaining, primary antibodies included anti-mouse MMP-2, -7, -9 and -12 (Chemicon, Temecula, CA), anti-smooth muscle α-actin (Sigma), anti-CD31 (BD Pharmingen, San Jose, CA), and F4/80 (Invitrogen, Carlsbad, CA). Isotype-matched antibodies were used as controls. Nuclei were detected with DAPI. The slides were photographed with a fluorescent microscope equipped with a digital camera (Zeiss, Maple Grove, MN).

Zymography

In situ gelatinase zymography was performed using EnzCheck Gelatinase Assay Kit (Molecular Probes, Eugene, OR) according to manufacturer's instructions with minor modification. Briefly, 5 μm-thick frozen section was incubated with buffer (50 mM Tris-HCl, 150 mM NaCl, 5 mM $CaCl_2$, 0.2 mM Sodium azide, pH 7.6) in the presence or absence of MMP inhibitor (10 mM 1,10-phenanthroline) for 15 minutes at 37°C. Next, DQ gelatin solution (0.1mg/ml in phosphate-buffered saline) and DAPI were added and the sections were incubated at 37°C for 60 minutes. The slides were photographed using a fluorescent microscope equipped with digital camera.

MMP activity of protein extracts was assessed using Fluorimetric "SensoLyte™ 520 Generic MMP Assay Kit" (AnaSpec, San Jose, CA) according to manufacturer's instructions. This kit detects the activity of several MMPs including MMP-1 to -14. Total protein was extracted from carotid arteries using lysis buffer [Tris-HCl 50mM, pH 7.4, NaCl 300 mM, Triton X-100 1%, and EDTA-free protease inhibitor cocktail (Roche, Indianapolis, IN)]. MMP activity was quantified by measuring fluorescence intensity after one hour at 37°C, and is presented as background corrected fluorescence intensity per μg of protein. The performance of the kit, which was used within its linear range, was validated in preliminary studies using recombinant active MMP-9 (not shown).

Quantitative reverse transcription polymerase chain reaction (RT-PCR)

Total RNA was isolated from carotid arteries using Absolutely RNA® Nanoprep Kit (Stratagene, La Jolla, CA), and reverse transcribed using QuanTitect® Reverse Tracsription Kit (QIAGEN, Valencia, CA). Quantitative PCR was performed on this cDNA in triplicates using Taqman® primers (Applied Biosystems, Foster City, CA) and an Applied Biosystems 7500 Real-Time PCR System following the manufacturer's instructions. The specificity of PCR amplifications was confirmed by running PCR products on agarose gels. The results were normalized to Glyceraldehyde 3-phosphate dehydrogenase (GAPDH). The following primer sets were used: MMP-2 (Mm00439506_m1), MMP-3, (Mm00440295_m1), MMP-9, (Mm00442991_m1), MMP-12, (Mm00500554_m1), MMP-13, (Mm01168713_m1) and GAPDH (Mm99999915_g1).

Imaging

Thirty seven (± 1.12) MBq RP782 (^{111}In-labeled) (11) was administered to groups of animals at 2, 4, and 8 weeks after $CaCl_2$ exposure through a right jugular vein intravenous

catheter. Animals were imaged after 2 hours on a high-resolution small animal imaging system (X-SPECT, Gamma Medica-Ideas, Northridge, CA) with 1-mm medium-energy collimators (12). Anesthetized mice (under Isoflurane) were placed in a fixed position on the animal bed. Three point sources of known activities (37 to 185 kBq) were placed in the field of view but outside the body to quantify uptake and to verify the accuracy of image fusion. The following acquisition parameters were used for microSPECT imaging: 360 degree, 128 projections, 30 seconds/projection (~80 minute image acquisition), with 174 and 242 keV photopeaks ±10% window (for ^{111}In). After completion of microSPECT imaging, animals were injected with a continuous infusion of iodinated CT contrast (iohexol 100 μL/min) over 2 minutes, and CT imaging was performed (energy 75 kVp/280 μA, matrix 512×512) to identify anatomic structure. The imaging protocol lasted ~1.5 hour, after which (3.5 hours after tracer administration) different tissues were harvested for autoradiography or gamma-well counting. To establish imaging specificity, 50-fold excess unlabeled precursor was administered to a group of animals 15 minutes prior to RP782 administration. For longitudinal imaging experiments, a group of animals (n=11) underwent repeated imaging with RP805 (^{99}Tc-labeled) (11) at 2 and 4 weeks. Fenestra (200μl, ART Advanced Research Technologies, Montreal, QC, Canada) was used as the CT contract agent in this group. The imaging protocol was similar to RP782 with the exception of the low-energy pinhole collimators and 140 Kev photopeak ±10% window used for ^{99m}Tc imaging. RP805 images were in general of better visual quality than those obtained using ^{111}In-labeled RP782, although we did not detect any quantitative difference in carotid uptake between the two tracers. For quantitative analysis of tracer uptake, cylindrical regions of interest (ROIs) were drawn at the level of carotid artery bifurcation (2×2×2 mm). A ROI immediately posterior to both carotids was used to calculate the background activity. Data were expressed as background-corrected cpv/MBq injected.

Autoradiography and gamma-well counting

A group of harvested carotid arteries were exposed to high-sensitivity, X-radiographic X-OMAT Kodak Scientific Imaging Film (Eastman Kodak, Rochester, NY) for various times to optimize detection. A set of standards with known activity deposited on Whatman paper (Whatman/GE Healthcare, Florham Park, NJ) was used to ascertain linearity of the signal. Other carotids were used for quantifying tracer uptake by gamma-well counting. Given their small size, the carotids could not be accurately weighed. Therefore, 3 mm sections of the artery proximal to carotid bifurcation were used for uptake measurements. Data were background and decay corrected and expressed as cpm/MBq injected.

MMP specificity assay

Five μm-thick sections of the left carotid artery at 4 weeks after surgery were incubated with 1,10-phenanthroline, a broad-spectrum MMP inhibitor (10 mM; Invitrogen, San Diego, CA), or control buffer for 15 minutes at 37°C. Next, RP782 (37.0 kBq) was added to tissues for 30 minutes at 37°C. After 3 washes the samples were transferred to a tube for gamma counting.

Statistical Analysis

Statistical analysis was performed using GraphPad Prism. Data are presented as mean ± standard error (SE). Differences between two groups are tested using two-tailed unpaired Student's *t* test, paired *t* test, or paired *t* test after logarithmic transformation for non-parametric data (ratio *t* test), as indicated. Multiple groups are compared using one way ANOVA (for parametric data) or Kruskal-Wallis test (for non-parametric data), followed by respectively, Tukey's or Dunn's post-hoc analysis. The non-parametric Spearman or the parametric Pearson correlation were used to test the association between 2 variables, as indicated. Significance was set at the 0.05 level.

Results

Carotid aneurysm in the apoE$^{-/-}$ mouse

Arterial aneurysm was induced by exposing the left common carotid arteries of high cholesterol-fed apoE$^{-/-}$ mice to $CaCl_2$. This led to progressive expansion of the artery over a period of 8 weeks (Figure 1A). Elastic van Gieson staining demonstrated straightening of elastic laminae and areas of discontinuity at 2 weeks that progressed to almost complete dissolution of the membranes by 8 weeks. The cross-sectional area of left carotid arteries was significantly higher than that of the saline-treated, control right carotid arteries at 2 weeks (0.26±0.05 mm^2 versus 0.10±0.01 mm^2, n=9, p=0.01), 4 weeks (0.30±0.03 mm^2 versus 0.09±0.01 mm^2, n=13, p<0.001) and 8 weeks (0.55±0.11 mm^2 versus 0.12±0.01 mm^2, n=10, p<0.01) after surgery (Figure 1B).

CD31 immunofluorescent staining confirmed the presence of a relatively preserved endothelium surrounding the lumen in aneurysmal (left) carotid arteries at 4 weeks after surgery (Suppl. Fig. 1). A number of neovessels were detectable in the adventitia. α-actin staining demonstrated the presence of medial VSMCs in the vicinity of the endothelial layer. A large number of macrophages (detected by F4/80 antibody staining) were present in aneurysmal arteries, but few, if any could be detected in control arteries (Suppl. Fig. 1).

MMP expression and activation in carotid aneurysm

MMPs play a key role in the development of aneurysm. Therefore, we assessed the expression of several vascular MMPs, including gelatinases and elastase (6) in carotid aneurysm. MMP-2 and -9 were detectable in aneurysmal arteries and exhibited a diffuse staining pattern consistent with their secreted nature (Figure 2A). A similar staining pattern was observed for two MMPs with elastase activity, MMP -7 and -12 (Suppl. Fig. 2). The temporal pattern of MMP expression was addressed by quantitative RT-PCR, and was found to vary among different MMPs (Suppl. Fig. 3). MMP-2 expression was rapidly upregulated after $CaCl_2$ application and reached the maximal level at 2 weeks, while MMP-9 expression peaked at 4 weeks. Similarly, MMP-3 expression increased with time and reached its maximal level at 4 weeks. MMP-12 and MMP-13 expression demonstrated a gradual and late induction reaching their maximal levels at 8 weeks after surgery.

In addition to expression level, MMP activation state and the level of inhibitors present regulate MMP activity. Therefore, we assessed MMP protease activity in the vessel wall by gelatinase in situ zymography at 4 weeks (Figure 2B). Gelatinase activity was present in a diffuse pattern in aneurysmal carotid arteries, while sham-operated arteries exhibited minimal activity. MMP-specificity of this protease activity was established by its marked reduction in the presence of a specific inhibitor, 1,10-phenanthroline. As a prelude to imaging studies, MMP activity in the vessel wall at different time points after surgery was quantified using a generic MMP activity assay. Compared to control carotid arteries, MMP activity in the left carotid artery was significantly higher in $CaCl_2$-treated left carotid arteries at 2 weeks (0.40±0.11 vs 0.09±0.02 arbitrary units, n=5. P<0.05), 4 weeks (0.68±0.13 vs 0.06±0.02 arbitrary units, n=8, P<0.01) and 8 weeks (0.28±0.04 vs 0.07±0.01 arbitrary units n=4, P<0.01) after surgery (Figure 2C).

MicroSPECT/CT Imaging of MMP Activation in Arterial Aneurysm

RP782, an ^{111}In-labeled tracer targeting the MMP activation epitope (11) was used to detect and quantify MMP activation by scintigraphic imaging in apoE$^{-/-}$ mice at 2, 4, or 8 weeks after surgery. MicroSPECT imaging was followed by CT angiography to localize carotid arteries. On microSPECT/CT images, RP782 signal was clearly detectable in aneurysmal, but not control, carotid arteries (Figure 3A, and supplemental movie 1). Imaging-derived

quantitative analysis of tracer uptake demonstrated a significant difference in target-to-background activity between the aneurysmal (left) and control (right) carotid arteries (2.44±0.09 and 1.29±0.02 respectively for left and right carotid arteries, n= 51, p<0.001). Background-corrected tracer uptake in the left carotid artery peaked at 4 weeks after surgery and was significantly higher than the uptake in the right carotid artery at each time point studied (2 weeks: 0.81±0.04 versus 0.23±0.02 cpv/MBq, n=16, p<0.001, 4 weeks: 1.58±0.14 versus 0.24±0.02 cpv/MBq, n=18, p<0.001, and 8 weeks: 1.32±0.12 versus 0.22±0.02 cpv/MBq, n=17, p<0.001 (Figure 3B). In some of the animals, RP782 signal was also visible at the surgical site.

Increased RP782 uptake in aneurysmal arteries was confirmed by ex vivo autoradiography, which consistently showed higher activity in the aneurysmal left, as compared to control, right carotid artery (Figure 4A). Tracer uptake in carotid arteries was further quantified by gamma-well counting in a sub-group of animals. Consistent with in vivo imaging results, left carotid artery uptake peaked at 4 week and was significantly higher than uptake in control, right carotid arteries (2 weeks: 870±160 versus 88±11 cpm/MBq, n=8, p<0.001, 4 weeks: 1251±367 versus 103±33 cpm/MBq, n=9, p<0.001, and 8 weeks: 445±56 versus 84±15 cpm/MBq, n=9, p<0.001, Figure 4B). There was an excellent correlation between in-vivo and ex-vivo quantification of carotid uptake (Pearson's r=0.77, p=0.001), establishing the validity of in vivo measurements for the following longitudinal studies. Furthermore, RP782 uptake significantly correlated with MMP activity assessed by quantitative zymography (Spearman's r=0.89, p=0.01, Figure 4C).

Specificity

The specificity of RP782 uptake in aneurysmal arteries was addressed in a group of animals at 4 weeks after surgery. Administration of 50-fold excess non-labeled precursor significantly reduced left carotid RP782 uptake detected by microSPECT/CT imaging in vivo (from 1.58±0.13 cpv/MBq, n=18 to 0.09±0.07 cpv/MBq, n=2, p<0.01, Figure 5A and B and supplemental movie 2). The blocking effect of non-labeled precursor on tracer uptake in the aneurysm (and non-aneursmal arteries) was clearly visible on carotid autoradiography (Suppl. Fig. 4). A broad-spectrum MMP inhibitor, 1,10-phenanthroline, significantly inhibited ex vivo RP782 binding to carotid aneurysm (from 3.2±0.6 cpm/KBq to 0.4±0.2 cpm/KBq, n=6, p<0.05, (Suppl. Fig. 5), further confirming the MMP-specificity of RP782 uptake in this model.

MMP activation and aneurysm expansion

Given the causal role of MMP activation in the pathogenesis of aneurysm, we sought to establish whether quantitation of MMP activation by scintigraphic imaging can provide information on subsequent aneurysm size in individual animals. In a longitudinal study, we sequentially imaged a group of animals at 2 and 4 weeks after surgery, following which the carotid arteries were harvested for morphometric analysis. We found no significant correlation between tracer uptake and aneurysm size at 4 weeks (data not shown). However, MMP tracer uptake at 2 weeks significantly correlated with the aneurysm size at 4 weeks (Pearson's r=0.69, n=11, p=0.02) (Figure 6).

Discussion

Arterial aneurysm affects various vascular beds and is an important cause of morbidity and mortality in most countries, including the US where abdominal aortic aneurysm (AAA) alone, is responsible for ~15,000 to 30,000 deaths every year (16,17). The high prevalence of aneurysm and the morbidity of its complications have led to institution of national screening programs in high risk populations (e.g., middle-aged men with a smoking history)

(3,18). Existing aneurysm imaging modalities (ultrasonography, CT and MRI) provide little information beyond the artery size. Although size is a good predictor of an aneurysm's risk of rupture and dissection, a large number of complications occur in smaller aneurysms that do not meet the clinical and imaging criteria for surgical repair (4,5,19). Rapid expansion of aneurysm increases the risk of rupture and dissection. However, at the present time, aneurysm expansion can only be detected retrospectively through serial imaging. Molecular imaging targeted at relevant molecular and cellular features of aneurysm can potentially address the limitations of existing imaging modalities, help identify patients at high risk for complications, and provide novel opportunities to study aneurysm biology in longitudinal studies.

In aneurysm, the imbalance between matrix synthesis and degradation, and cell proliferation and death creates an arterial wall with reduced tensile strength which is prone to expansion, rupture or dissection under the influence of hemodynamic forces. Vessel wall inflammation plays a key role in this process (20). Inflammatory and other vascular cells produce high levels of activated proteases, including MMPs, which through digestion of collagen and elastin participate in the weakening of the vessel wall and facilitate recruitment of additional inflammatory cells (21). Cytokines, reactive oxygen species, prostaglandin derivatives and other mediators released by inflammatory cells induce VSMC death and media hypotrophy and adversely affect the ability of VSMCs to repair the matrix scaffold (22). As such, complicated aneurysms commonly contain a high density of inflammatory cells in conjunction with high levels of activated proteases, including MMPs (7,17,21). A similar pattern is observed in various experimental animal models of aneurysm, all of which replicate within a few weeks a process that normally takes years to develop in humans. The $CaCl_2$ model mimics many features of human disease and has been extensively used to study the molecular mechanisms of aneurysm formation (23–25).

Based on this view of pathogenesis, imaging MMP activation in the vessel wall appears as a promising approach to identifying aneurysms that are prone to expansion. MMPs are a multi-gene family of at least 23 secreted or transmembrane zinc- and calcium-dependent endopeptidases that selectively digest individual components of extracellular matrix and other proteins, and play a key role in vascular remodeling (6,10). MMPs causal role in the expansion of aneurysm is supported by several lines of evidence. Histological studies demonstrate differences in MMP expression and activity between normal artery and aneurysms of different sizes or those ruptured (7,26,27). Targeted disruption of specific members of the MMP family reduces aneurysm formation in animal models (8,9,28,29). MMP inhibitors (e.g., doxycycline) inhibit aneurysm formation in animal models, a finding that has raised the possibility of treating MMP expansion in humans using similar agents (8). Expression, activation, and inhibition by tissue inhibitors of matrix metalloproteinases (TIMPs) are the main regulatory mechanisms of MMP activity. MMPs are biosynthesized either as secreted or transmembrane proenzymes. Activation of these latent MMPs is achieved through enzymatic cleavage of the propeptide which exposes a common catalytic domain (10). Several broad spectrum MMP inhibitors bind to, and inactivate this domain. Tracers used in this study are structurally based on broad spectrum MMP inhibitors and bind with high specificity to the exposed catalytic domain (11,13). This enabled us to simultaneously detect activation of several MMPs by molecular imaging in vivo. As MMP activation is a common pathophysiological feature of aneurysm in different arterial beds, we focused on imaging carotid arteries to circumvent technical challenges associated with imaging aorta in the mouse, where the proximity to the bladder and kidneys complicates signal detection and quantification. We demonstrated that MMP activation can be imaged as early as 2 weeks, and peaks at 4 weeks in this murine model of aneurysm. Tracer uptake in the surgical wound was a confounding factor which was dealt with by localizing the target arteries by CT angiography. Ex vivo assessment of tracer uptake by gamma well counting

further confirmed that the tracer localizes in the aneurysm. The target to background ratio in the aneurysm was sufficient for microSPECT imaging of carotid aneurysm in the mouse. It remains to be empirically determined whether high enough ratios for imaging can be obtained with human aneurysm.

The data on MMP plasma levels and aneurysm growth are inconclusive (30). This may be explained by the fact that beside MMP expression in the aneurysm, MMP plasma levels may be influenced by other factors. In normal arteries MMP-2, TIMP-1 and TIMP-2 are produced constitutively by endothelial cells and VSMCs, but no in situ enzymatic activity is detectable (6). Here, we demonstrated that in addition to MMP-2 and MMP-9, which play an important role in the development of aneurysm (9), other MMPs (including MMP-3, -12, and -13) are also upregulated in aneurysm. Major differences were detected in the time course of MMP expression, suggesting that each MMP plays a distinct role in the pathogenesis. There is no established method for detecting focal activation of specific MMPs in vivo. Using a tracer with specificity for the MMP activation epitope we were able to simultaneously detect activation of multiple MMPs, and demonstrated that this approach can be used to predict the subsequent aneurysm size. Tracers targeted at individual members of the MMP family are in development (31–33). Given major differences in the expression pattern of different MMPs and lack of experimental data on their activation, it remains to be empirically determined if in vivo imaging of any specific member of the MMP family will provide more robust information on an aneurysm's propensity to expansion.

A non-specific marker of inflammation, ^{18}F-fluorodeoxyglucose (FDG) has been assessed for detection of inflammation and propensity to complications in human studies (34–36) and found to be of insufficient sensitivity and specificity (37). MMP imaging, used previously by our group (12) and others (13,38,39) to image MMP activation in injury-induced vascular remodeling and atherosclerosis, targets a process directly linked to extracellular matrix remodeling. With its potentially better specificity for remodeling, it appears as a promising alternative approach to imaging aneurysm biology. However, it remains to be empirically determined whether this approach has a better specificity and sensitivity than FDG. The quantitative nature of scintigraphic imaging allowed us to accurately quantify tracer uptake in carotid arteries. Not unexpectedly, there was no significant correlation between RP782 uptake and expression of each specific member of the MMP family (data not shown). In the absence of a better alternative, we relied on a generic MMP substrate to assess MMP activation and correlate it with RP782 uptake. Despite differences in relative affinity of individual MMPs for RP782 and this substrate, we detected a strong correlation between these two independent measures of MMP activation. Finally, while MMP activation detected by scintigraphic imaging and aneurysm size at 4 weeks did not correlate, tracer uptake at 2 weeks correlated well with the aneurysm size at 4 weeks, establishing MMP-targeted molecular imaging as a tool for predicting future expansion of aneurysm.

Conclusion

MMP-targeted imaging provides a tool for studying aneurysm biology, its prognosis and response to therapy. It remains to be empirically determined if other molecular and cellular targets (e.g., specific MMPs, or other proteases) can serve as alternative or complementary approaches to MMP-targeted imaging of aneurysm biology. Ultimately, prospective identification of aneurysms that are prone to expansion will help identify and treat these high risk aneurysms and potentially reduce aneurysm morbidity and mortality.

Supplementary Material

Refer to Web version on PubMed Central for supplementary material.

Acknowledgments

This work was supported by National Institutes of Health R01 HL85093, Program Project HL70295, and a Department of Veterans Affairs Merit Award to Mehran M. Sadeghi. Jiasheng Zhang received a research award for this work from the American Society of Nuclear Cardiology.

References

1. Davies MJ. Aortic aneurysm formation: lessons from human studies and experimental models. Circulation Jul 21;1998 98(3):193–195. [PubMed: 9697816]
2. El-Hamamsy I, Yacoub MH. Cellular and molecular mechanisms of thoracic aortic aneurysms. Nat Rev Cardiol Dec;2009 6(12):771–786. [PubMed: 19884902]
3. Cosford PA, Leng GC. Screening for abdominal aortic aneurysm. Cochrane Database Syst Rev 2007;(2):CD002945. [PubMed: 17443519]
4. Ashton HA, Buxton MJ, Day NE, et al. The Multicentre Aneurysm Screening Study (MASS) into the effect of abdominal aortic aneurysm screening on mortality in men: a randomised controlled trial. Lancet Nov 16;2002 360(9345):1531–1539. [PubMed: 12443589]
5. Lederle FA, Wilson SE, Johnson GR, et al. Immediate repair compared with surveillance of small abdominal aortic aneurysms. N Engl J Med May 9;2002 346(19):1437–1444. [PubMed: 12000813]
6. Galis ZS, Khatri JJ. Matrix metalloproteinases in vascular remodeling and atherogenesis: the good, the bad, and the ugly. Circ Res Feb 22;2002 90(3):251–262. [PubMed: 11861412]
7. Thompson RW, Holmes DR, Mertens RA, et al. Production and localization of 92-kilodalton gelatinase in abdominal aortic aneurysms. An elastolytic metalloproteinase expressed by aneurysm-infiltrating macrophages. J Clin Invest Jul;1995 96(1):318–326. [PubMed: 7615801]
8. Pyo R, Lee JK, Shipley JM, et al. Targeted gene disruption of matrix metalloproteinase-9 (gelatinase B) suppresses development of experimental abdominal aortic aneurysms. J Clin Invest Jun;2000 105(11):1641–1649. [PubMed: 10841523]
9. Longo GM, Xiong W, Greiner TC, Zhao Y, Fiotti N, Baxter BT. Matrix metalloproteinases 2 and 9 work in concert to produce aortic aneurysms. J Clin Invest Sep;2002 110(5):625–632. [PubMed: 12208863]
10. Visse R, Nagase H. Matrix metalloproteinases and tissue inhibitors of metalloproteinases: structure, function, and biochemistry. Circ Res May 2;2003 92(8):827–839. [PubMed: 12730128]
11. Su H, Spinale FG, Dobrucki LW, et al. Noninvasive targeted imaging of matrix metalloproteinase activation in a murine model of postinfarction remodeling. Circulation Nov 15;2005 112(20): 3157–3167. [PubMed: 16275862]
12. Zhang J, Nie L, Razavian M, et al. Molecular imaging of activated matrix metalloproteinases in vascular remodeling. Circulation Nov 4;2008 118(19):1953–1960. [PubMed: 18936327]
13. Fujimoto S, Hartung D, Ohshima S, et al. Molecular imaging of matrix metalloproteinase in atherosclerotic lesions: resolution with dietary modification and statin therapy. J Am Coll Cardiol Dec 2;2008 52(23):1847–1857. [PubMed: 19038682]
14. Chiou AC, Chiu B, Pearce WH. Murine aortic aneurysm produced by periarterial application of calcium chloride. J Surg Res Aug;2001 99(2):371–376. [PubMed: 11469913]
15. Sadeghi MM, Krassilnikova S, Zhang J, et al. Detection of injury-induced vascular remodeling by targeting activated alphavbeta3 integrin in vivo. Circulation Jul 6;2004 110(1):84–90. [PubMed: 15210600]
16. Kent KC, Zwolak RM, Jaff MR, et al. Screening for abdominal aortic aneurysm: a consensus statement. J Vasc Surg Jan;2004 39(1):267–269. [PubMed: 14718853]
17. Ince H, Nienaber CA. Etiology, pathogenesis and management of thoracic aortic aneurysm. Nat Clin Pract Cardiovasc Med Aug;2007 4(8):418–427. [PubMed: 17653114]
18. Lederle FA. Screening for AAA in the USA. Scand J Surg 2008;97(2):139–141. [PubMed: 18575032]
19. Lederle FA, Johnson GR, Wilson SE, et al. The aneurysm detection and management study screening program: validation cohort and final results. Aneurysm Detection and Management

Veterans Affairs Cooperative Study Investigators. Arch Intern Med May 22;2000 160(10):1425–1430. [PubMed: 10826454]

20. Curci JA, Thompson RW. Adaptive cellular immunity in aortic aneurysms: cause, consequence, or context? J Clin Invest Jul;2004 114(2):168–171. [PubMed: 15254583]
21. Freestone T, Turner RJ, Coady A, Higman DJ, Greenhalgh RM, Powell JT. Inflammation and matrix metalloproteinases in the enlarging abdominal aortic aneurysm. Arterioscler Thromb Vasc Biol Aug;1995 15(8):1145–1151. [PubMed: 7627708]
22. Walton LJ, Franklin IJ, Bayston T, et al. Inhibition of prostaglandin E2 synthesis in abdominal aortic aneurysms: implications for smooth muscle cell viability, inflammatory processes, and the expansion of abdominal aortic aneurysms. Circulation Jul 6;1999 100(1):48–54. [PubMed: 10393680]
23. Xiong W, Knispel R, MacTaggart J, Greiner TC, Weiss SJ, Baxter BT. Membrane-type 1 matrix metalloproteinase regulates macrophage-dependent elastolytic activity and aneurysm formation in vivo. J Biol Chem Jan 16;2009 284(3):1765–1771. [PubMed: 19010778]
24. Yoshimura K, Aoki H, Ikeda Y, Furutani A, Hamano K, Matsuzaki M. Regression of abdominal aortic aneurysm by inhibition of c-Jun N-terminal kinase in mice. Ann N Y Acad Sci Nov;2006 1085:74–81. [PubMed: 17182924]
25. Xiong W, MacTaggart J, Knispel R, Worth J, Persidsky Y, Baxter BT. Blocking TNF-alpha attenuates aneurysm formation in a murine model. J Immunol Aug 15;2009 183(4):2741–2746. [PubMed: 19620291]
26. Taketani T, Imai Y, Morota T, et al. Altered patterns of gene expression specific to thoracic aortic aneurysms: microarray analysis of surgically resected specimens. Int Heart J Mar;2005 46(2):265–277. [PubMed: 15876810]
27. Wilson WR, Anderton M, Schwalbe EC, et al. Matrix metalloproteinase-8 and -9 are increased at the site of abdominal aortic aneurysm rupture. Circulation Jan 24;2006 113(3):438–445. [PubMed: 16432074]
28. Longo GM, Buda SJ, Fiotta N, et al. MMP-12 has a role in abdominal aortic aneurysms in mice. Surgery Apr;2005 137(4):457–462. [PubMed: 15800495]
29. Ikonomidis JS, Barbour JR, Amani Z, et al. Effects of deletion of the matrix metalloproteinase 9 gene on development of murine thoracic aortic aneurysms. Circulation Aug 30;2005 112(9 Suppl):I242–248. [PubMed: 16159824]
30. Golledge J, Tsao PS, Dalman RL, Norman PE. Circulating markers of abdominal aortic aneurysm presence and progression. Circulation Dec 2;2008 118(23):2382–2392. [PubMed: 19047592]
31. Lebel R, Jastrzebska B, Therriault H, et al. Novel solubility-switchable MRI agent allows the noninvasive detection of matrix metalloproteinase-2 activity in vivo in a mouse model. Magn Reson Med Nov;2008 60(5):1056–1065. [PubMed: 18956456]
32. Scherer RL, VanSaun MN, McIntyre JO, Matrisian LM. Optical imaging of matrix metalloproteinase-7 activity in vivo using a proteolytic nanobeacon. Mol Imaging May-Jun;2008 7(3):118–131. [PubMed: 19123982]
33. Watkins GA, Jones EF, Scott Shell M, et al. Development of an optimized activatable MMP-14 targeted SPECT imaging probe. Bioorg Med Chem Jan 15;2009 17(2):653–659. [PubMed: 19109023]
34. Sakalihasan N, Van Damme H, Gomez P, et al. Positron emission tomography (PET) evaluation of abdominal aortic aneurysm (AAA). Eur J Vasc Endovasc Surg May;2002 23(5):431–436. [PubMed: 12027471]
35. Kotze CW, Menezes LJ, Endozo R, Groves AM, Ell PJ, Yusuf SW. Increased metabolic activity in abdominal aortic aneurysm detected by 18F-fluorodeoxyglucose (18F-FDG) positron emission tomography/computed tomography (PET/CT). Eur J Vasc Endovasc Surg Jul;2009 38(1):93–99. [PubMed: 19217326]
36. Reeps C, Essler M, Pelisek J, Seidl S, Eckstein HH, Krause BJ. Increased 18F-fluorodeoxyglucose uptake in abdominal aortic aneurysms in positron emission/computed tomography is associated with inflammation, aortic wall instability, and acute symptoms. J Vasc Surg Aug;2008 48(2):417–423. discussion 424. [PubMed: 18572354]

37. Kuehl H, Eggebrecht H, Boes T, et al. Detection of inflammation in patients with acute aortic syndrome: comparison of FDG-PET/CT imaging and serological markers of inflammation. Heart Nov;2008 94(11):1472–1477. [PubMed: 18070949]

38. Schafers M, Riemann B, Kopka K, et al. Scintigraphic imaging of matrix metalloproteinase activity in the arterial wall in vivo. Circulation Jun 1;2004 109(21):2554–2559. [PubMed: 15123523]

39. Ohshima S, Petrov A, Fujimoto S, et al. Molecular imaging of matrix metalloproteinase expression in atherosclerotic plaques of mice deficient in apolipoprotein e or low-density-lipoprotein receptor. J Nucl Med Apr;2009 50(4):612–617. [PubMed: 19289429]

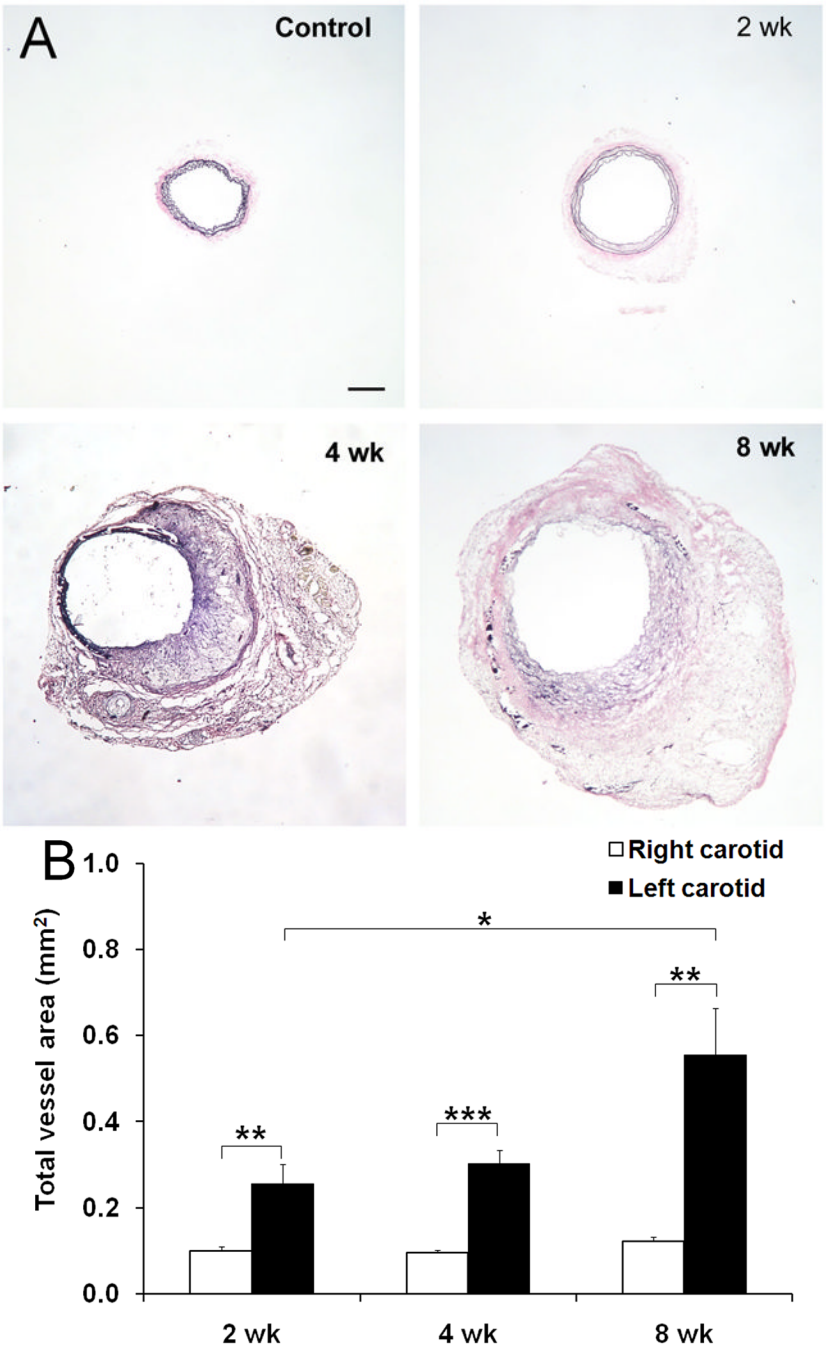

Figure 1.

Carotid aneurysm in apoE$^{-/-}$ mice. (A) Representative examples of elastic van Gieson staining of common carotid artery exposed to NaCl (control) or at 2, 4 and 8 weeks (wk) after exposure to $CaCl_2$, demonstrating marked enlargement of the artery. Scale bar: 100 μm. (B) Morphometric analysis of the total vessel area following exposure of left carotid artery to $CaCl_2$. n=9–13 in each group, * $p<0.05$, ** $p=0.01$, *** $p<0.001$.

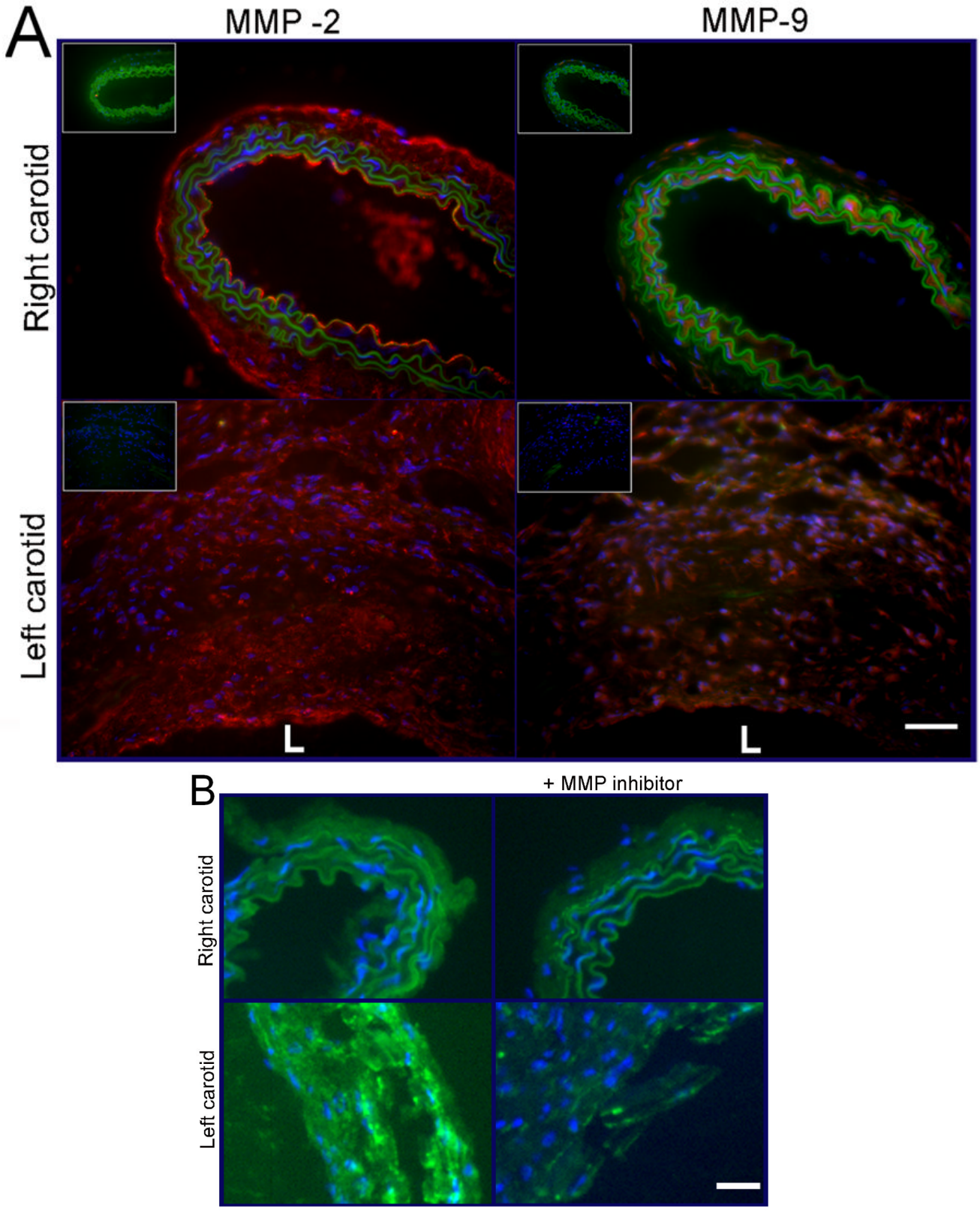

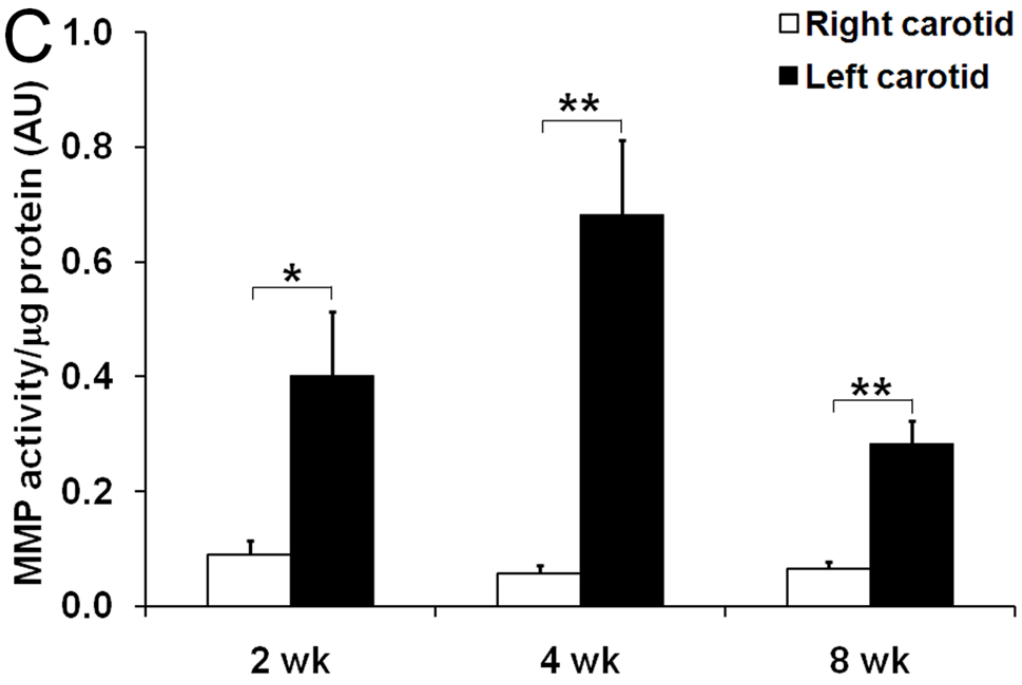

Figure 2.

MMP expression and activity in aneurysm. (A) Representative examples of MMP-2 and MMP-9 immunofluorescent staining (in red) of carotid arteries at 4 weeks, demonstrating diffuse MMP expression in the aneurismal left carotid artery. Elastic membranes are detected by their auto-fluorescence in green. Nuclei are detected by DAPI in blue. Insets represent staining with control antibodies. L: lumen. Scale bar: 100 μm. (B) Examples of in situ gelatinase zymography of control right and aneurysmal left carotid arteries at 4 weeks. Protease activity is markedly reduced in the presence of a specific MMP inhibitors, 1,10-phenanthroline. Nuclei are detected by DAPI in blue. Scale bar: 20 μm. (C) MMP activity quantified using a generic fluorogenic assay at 2, 4 and 8 weeks after $CaCl_2$ application. n=9–13. * $p<0.05$, ** $p<0.01$. AU: Arbitrary Units.

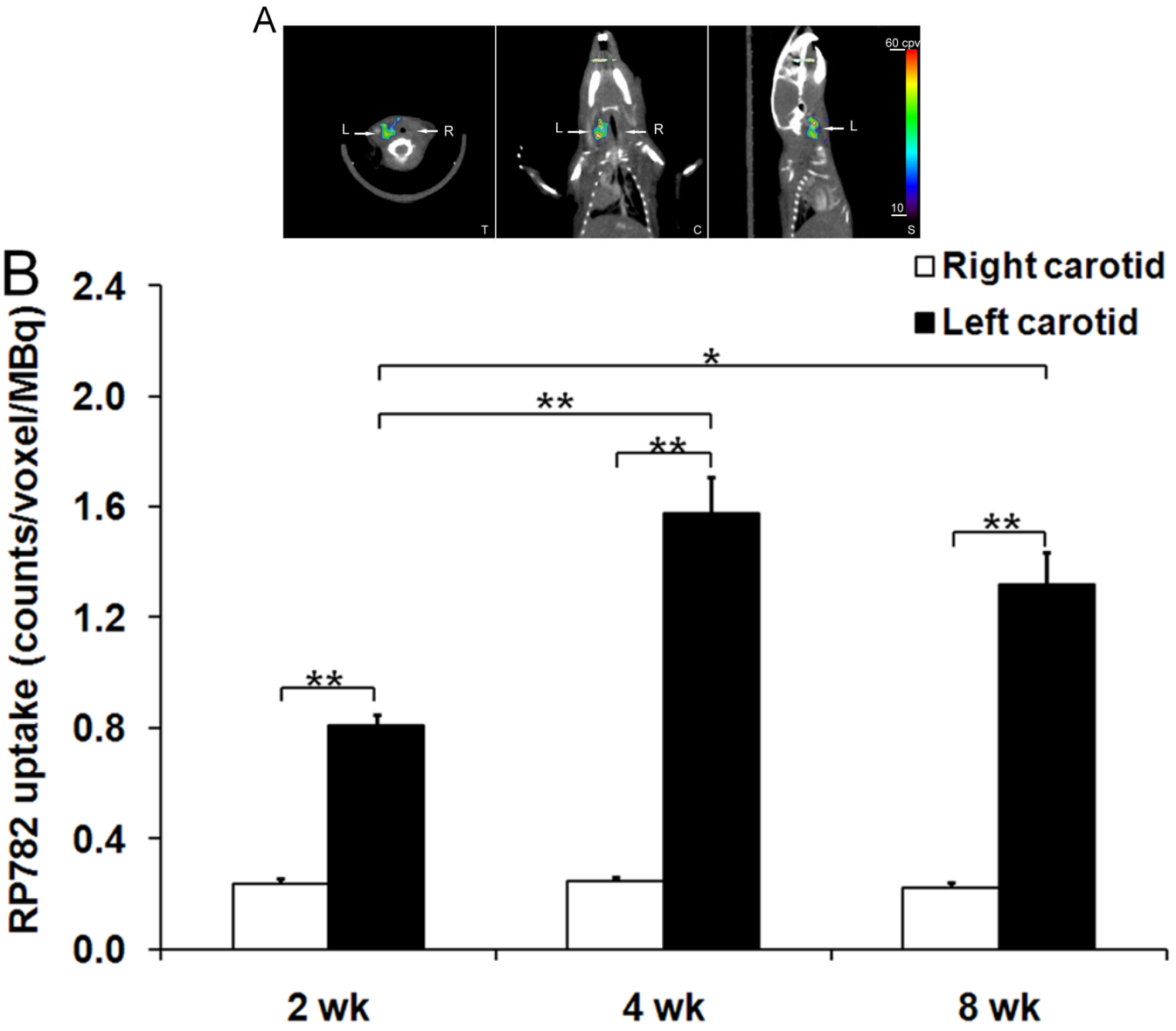

Figure 3.

In vivo imaging of MMP activation in aneurysm. (A) An example of fused microSPECT/CT images of a mouse 4 weeks after surgery to induce carotid aneurysm. Arrows point to aneurysmal left (L) and control right (R) carotid arteries. S indicates sagittal, C, coronal, and T, transverse slices, cpv, counts per voxel. (B) Image-derived quantitative analysis of background-corrected RP782 carotid uptake. Background-corrected tracer uptake in the left carotid artery peaked at 4 weeks (wk) after surgery and was significantly higher than uptake in the right carotid artery at every time point studied. n=16–18 in each group, * p=0.01, ** p<0.001.

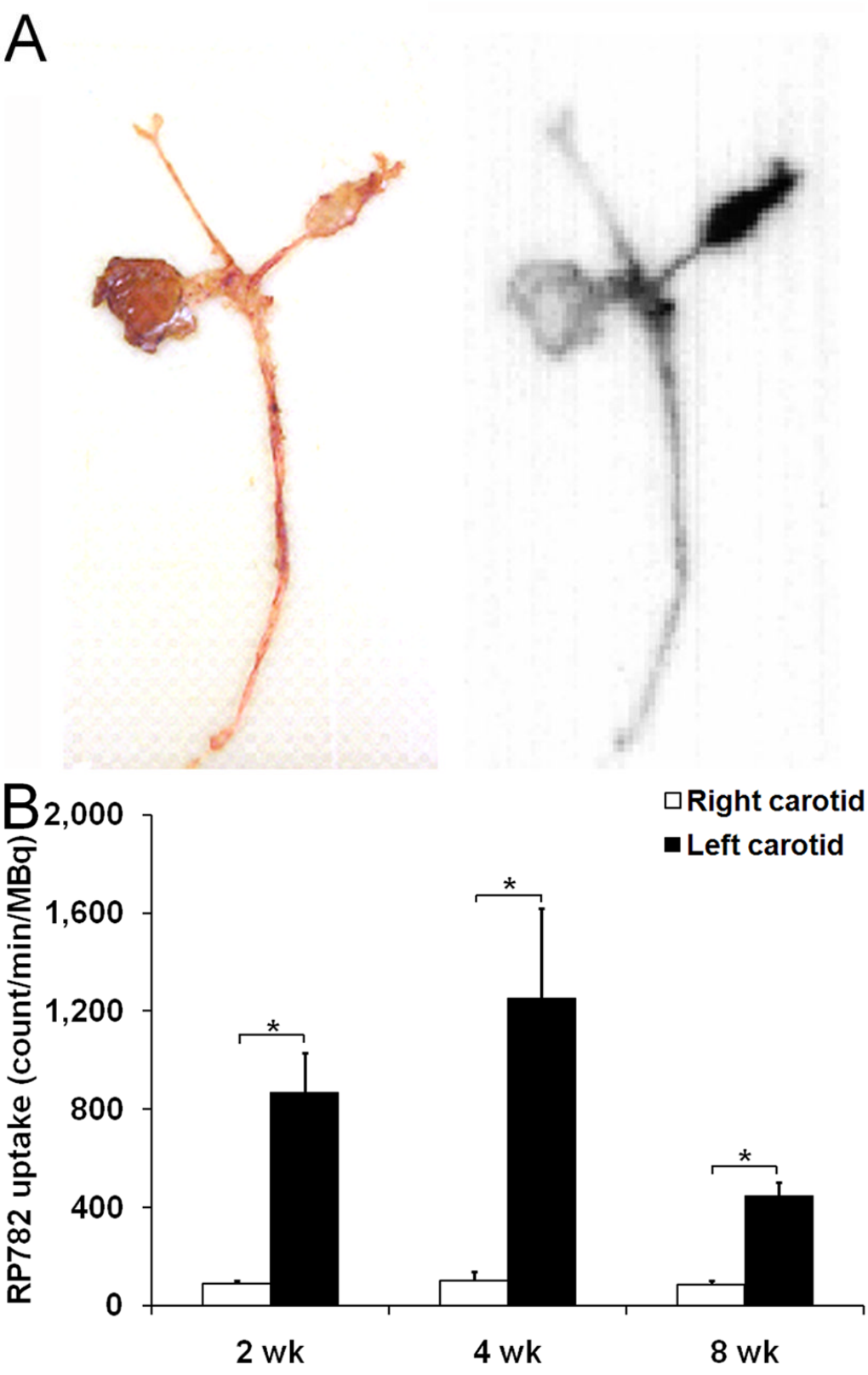

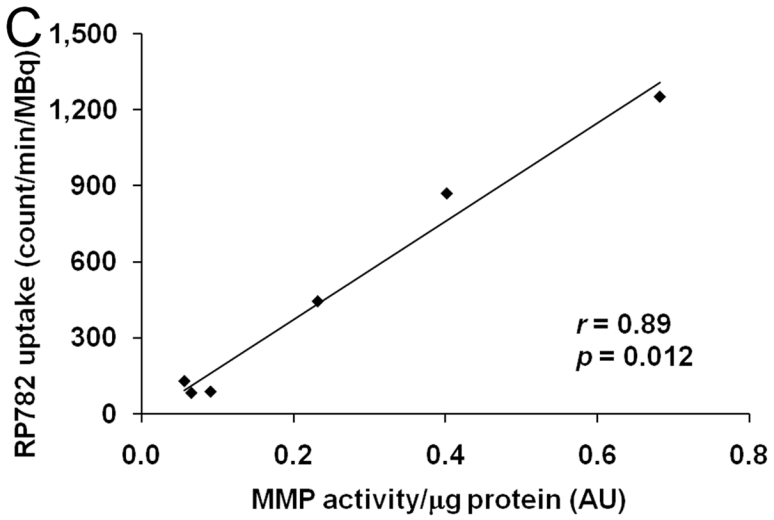

Figure 4.

Ex vivo analysis MMP tracer uptake in aneurysm. (A) An example of carotid arteries and aorta at 4 weeks after aneurysm induction, harvested and photographed following RP782 imaging (left panel), with corresponding autoradiography (right panel). The figure is representative of the data from at least 5 animals from each time point. (B) Quantitative analysis RP782 uptake by gamma-well counting. n=8–9 in each group. *p<0.001. (C), Correlation between carotid RP782 uptake and MMP activity assessed by quantitative zymography. Spearman's r=0.89, p=0.01. AU: Arbitrary Units.

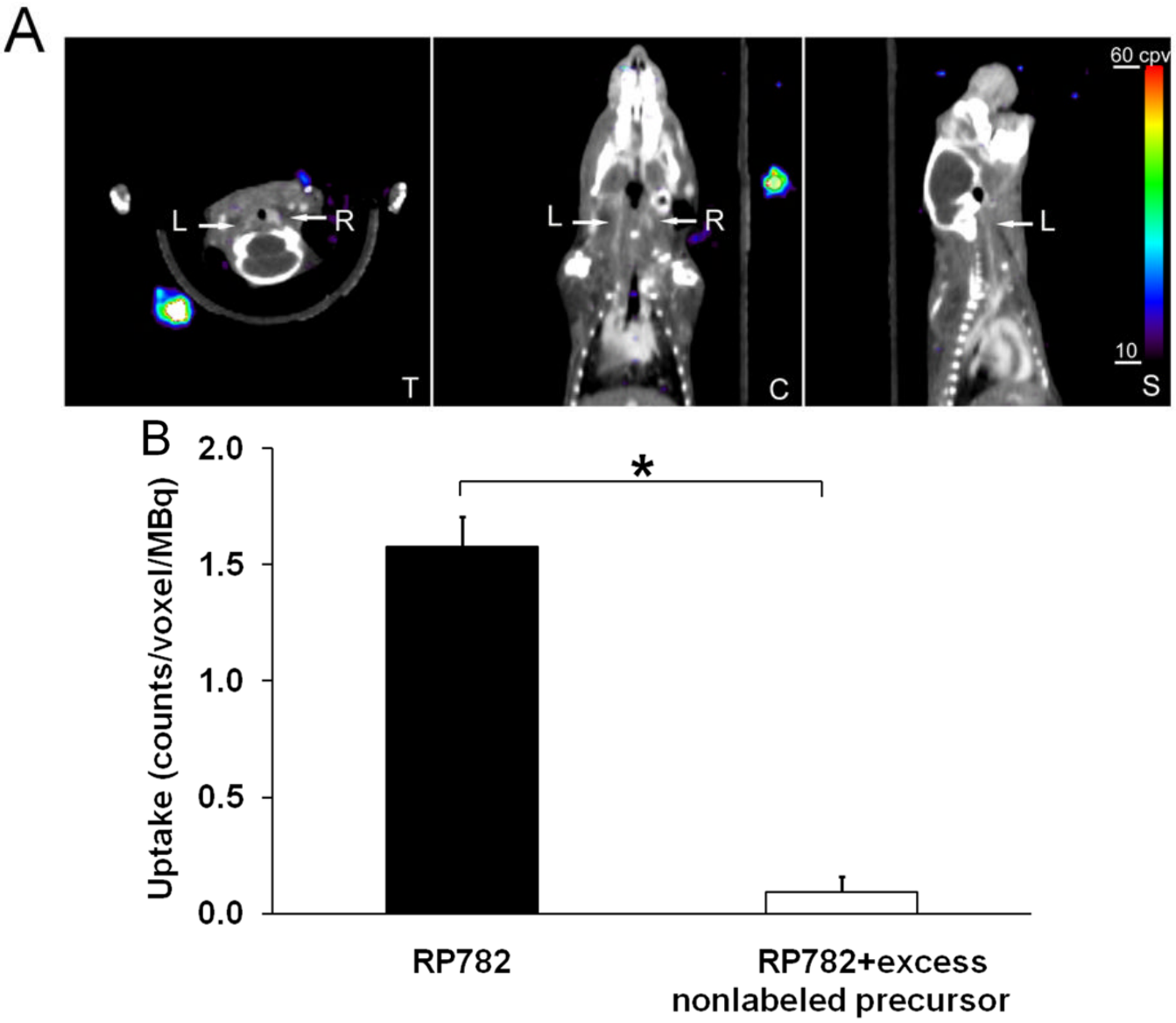

Figure 5.

MMP tracer uptake specificity. (A) An example of RP782 microSPECT/CT imaging following administration of 50-fold excess precursor in a mouse 4 weeks after surgery to induce carotid aneurysm. Arrows point to aneurysmal left (L) and control right (R) carotid arteries. S indicates sagittal, C, coronal, and T, transverse slices, cpv, counts per voxel. (B) Image-derived quantitative analysis of RP782 carotid uptake in the absence (n=18) or presence (n=2) of 50-fold excess non-labeled precursor. *p<0.01.

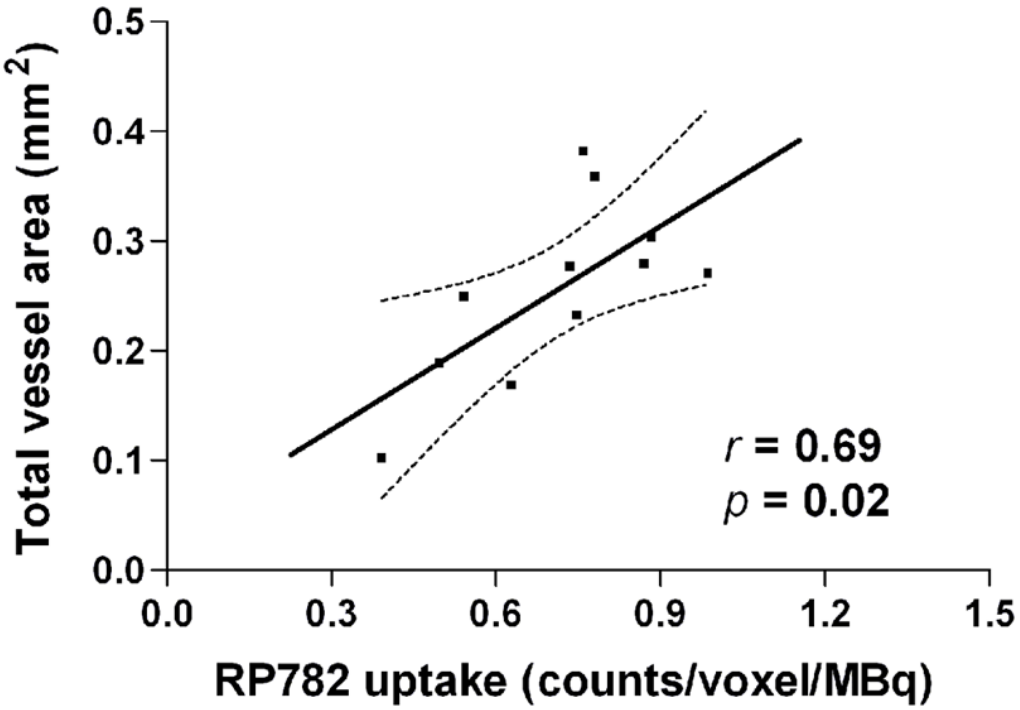

Figure 6.
MMP activation and aneurysm size. There is a significant correlation between MMP tracer uptake in aneurysmal carotid artery at 2 weeks and total vessel area measured at 4 weeks in the same animal. Pearson's r=0.69, n=11, p=0.02. Dotted lines represent 95% confidence interval.